Lab on a Chip

A Wearable Patch for Continuous Monitoring of Sweat Electrolytes during Moderate and Intense Exertion

Journal:	*Lab on a Chip*
Manuscript ID	LC-ART-05-2018-000510.R1
Article Type:	Paper
Date Submitted by the Author:	15-Jul-2018

Complete List of Authors:	Alizadeh, Azar; GE Global Research, Burns, Andrew; GE Global Research Lenigk, Ralf; GE Global Research Gettings, Rachel; General Electric - Global Research Center Ashe, Jeffrey; GE Global Research Porter, Adam; Dublin City University McCaul, mararet; Dublin City University Diamond, Dermot; Dublin City University, School of Chemical Sciences White, Paddy; Shimmer Inc. Skeath, Perry; University of Arizona, Center for Integrative Medicine, College of Medicine Tomczak, Melanie; UES Inc Barrett, Ruairi; Dublin City University Faculty of Science and Health

SCHOLARONE™
Manuscripts

A Wearable Patch for Continuous Monitoring of Sweat Electrolytes during Moderate and Intense Exertion

Azar Alizadeh[1], Andrew Burns, Ralf Lenigk, Rachel Gettings and Jeffrey Ashe (*GE Global Research, Niskayuna, NY, USA)*

Adam Porter, Margaret McCaul, Ruairi Barrett, Dermot Diamond (*Dublin City University, Dublin, Ireland*)

Paddy White (*Shimmer, DCU Alpha, Dublin, Ireland*)

Perry Skeath (University of Arizona, Tucson, AZ, USA)

Melanie Tomczak (UES, Dayton, OH, USA)

Abstract

Implementation of wearable sweat sensors for continuous measurement of fluid based biomarkers (including electrolytes, metabolites and proteins) is an attractive alternative to common, yet intrusive and invasive, practices such as urine or blood analysis. Recent years have witnessed several key demonstrations of sweat based electrochemical sensing in wearable formats, however, there are still significant challenges and opportunities in this space for clinical acceptance, and thus mass implementation of these devices. For instance, there are inherent challenges in establishing direct correlations between sweat-based and gold-standard plasma-based biomarker concentrations for clinical decision-making. In addition, the wearable sweat monitoring devices themselves may exacerbate these challenges, as they can significantly alter sweat physiology (example, sweat rate and composition). Reported here is the demonstration of a fully integrated, wireless, wearable and flexible sweat sensing device for non-obtrusive and continuous monitoring of electrolytes during moderate to intense exertion as a metric for hydration status. The focus of this work is twofold: 1- design of a conformable fluidics systems to suit conditions of operation for sweat collection (to minimize sensor lag) with rapid removal of sweat from the sensing site (to minimize effects on sweat physiology). 2- integration of Na^+ and K^+ ion-selective electrodes (ISEs) with flexible microfluidics and low noise small footprint electronics components to enable wireless, wearable sweat monitoring. While this device is specific to electrolyte analysis during intense perspiration, the lessons in microfluidics and overall system design are likely applicable across a broad range of analytes.

Introduction

Human performance monitoring and augmentation are emerging concepts to improve safety and effectiveness in the workplace, playing field and combat theater. Including information about the state of the human in diverse scenarios, ranging from factory environments to military operations, promises new capabilities regarding logistical decisions and increased protection for both human operators and physical assets. Prime environments for human performance monitoring are tasks where strenuous physical activity is a part of the daily routine (elite athletes, warfighters, emergency personnel, etc.). In circumstances where significant exertion is required, continuous monitoring of hydration and heat stress are crucial (but currently lacking) additions to monitoring physiological parameters such as heart rate, heart rate variability, motion, temperature, blood oxygenation, etc. Poor management of hydration status

[1] To whom correspondence should be addressed: alizadeh@ge.com

(both dehydration and hyperhydration) can lead to catastrophic medical events during exertion to the point of injury or death [1]. Increasing levels of dehydration have also been shown to cause impairments during exercise, where up to 10% performance decline is shown when levels of dehydration approach 3–4% of body mass loss [2]. Dehydration also adversely affects cognitive function and mood [3-6].

Currently, there are no high-resolution solutions for accurate, non-invasive and continuous assessment of hydration in field applications. Hydration is a complex physiological parameter and its assessment requires multiple complementary sensing modalities [7]. In order to develop a representative understanding of whole-body hydration, we must combine the outputs of multiple wearable sensor modalities to understand water content and fluid balance (intracellular vs. extracellular water), as well as sweat electrolyte composition. Laboratory gold standards for hydration assessment are based on total body water and plasma osmolality under controlled conditions of stable and equilibrated body fluids [8, 9]. In practice, nude body mass losses are used as an indirect measure of fluid content, but continuous assessment of an individual's nude body mass fluctuations in the field during a mission is unrealistic. Similarly, blood (or urine) osmolality measurements are intrusive and require sophisticated equipment and training for analysis. We have recently demonstrated in resting, healthy human subjects and in patients undergoing hemodialysis, that impedance tomography (layer-based impedance spectroscopy) can be very effective in tracking fluid changes at deep tissue levels, with minimal skin interferences [10, 11]. While impedance methods demonstrate high sensitivity to fluid changes, their specificity is confounded by factors that influence the electrical conductivity of fluid (e.g., electrolytes). Sweat is an easily accessible bio-fluid that contains multiple electrolytes (Na^+, K^+, etc.) along with other biomarkers such as glucose, lactate, cortisol, interleukins, etc. Thus, monitoring electrolyte concentration changes in sweat is attractive for dynamic hydration assessment in the field to guide fluid and electrolyte replacement strategies and control activity/exertion.

Recently, significant progress has been made towards the development of wearable sensing devices for non-invasive *in situ* monitoring of multiple sweat based biomarkers, including electrolytes, glucose, lactate and pH [12-23]. For example, Gui *et al*. have developed a fully integrated, wearable sensor system, allowing for simultaneous *in situ* analysis and wireless transmission of multiple sweat biomarkers [21]. Sonner *et al*. have developed sweat stimulation and sensing mechanisms that allow for continuous sweat monitoring even at rest (low perspiration rates) [12]. Rogers *et al*. have developed a highly compliant tattoo-like sweat patches with microfluidics for time-stamped colorimetric measurement of multiple sweat biomarkers and sweat rate [20]. Glennon *et al.* have developed a sampling platform that allows for rapid transport of sweat from the skin into device minimizing pooling and mixing of sweat [17]. Despite these impressive advances, there are still significant challenges and opportunities in wearable sweat sensing [24, 25]. A key challenge for clinical acceptance, and thus mass implementation of these devices, is establishing direct correlations between sweat and plasma biomarker concentrations.

There are inherent complexities in sweat monitoring and analysis due to several factors. Sweat rate and solute concentrations are highly individual and can change greatly within an individual over time, due to environment, acclimatization, diet or other factors including the type of exercise regimen [26, 27], regional variations in sweat rate across the body are well documented [28]. In addition to these inherent variabilities, sweat monitoring devices themselves may significantly alter sweat physiology (both sweat rate and composition). To capture sweat for analysis, these devices inherently prevent sweat evaporation and keep at least some sweat in contact with the skin. This prolonged exposure of skin to sweat can cause swelling of the epidermis with consequent blockage of the sweat ducts and decreases in sweat rate (hydromeiosis) [29, 30]. Additionally, sweat monitoring devices also require adhesives for skin attachment. Koh *et al*. have

observed anomalously high sweat rates in small collection areas, where adjacent adhesives blocking sweat glands may have led to compensatory sweating of adjacent glands in the sweat harvesting area [15].
To realize the potential of sweat sensing in hydration monitoring applications, further refinements in device design and reliability, as well as appropriate testing and control protocols that are adequate for the specific concept of operation are required. In this paper, we report on our work towards the development of a fully integrated, wireless, wearable and flexible sweat sensing device for non-obtrusive and continuous monitoring of electrolytes during moderate to intense exertion. The focus of this work is twofold: 1- design of a conformable fluidics systems to suit conditions of operation for sweat collection (to minimize sensor lag) with rapid removal of sweat from the sensing site (to minimize effects on sweat physiology). 2- integration of Na^+ and K^+ ion-selective electrodes (ISEs) with flexible microfluidic components to enable wireless, wearable sweat monitoring.

Of all the solutes in sweat, sodium is the most abundant and extensively studied. Sweat sodium concentration within the sweat gland begins nearly isotonic to plasma sodium (independent of sweat rate), but becomes hypotonic (relative to plasma) on its way to the skin surface due to sodium adsorption within the duct [31]. This reabsorption is limited by the rate and capacity limits of sweat ducts to re-absorb sodium, and thus, the sweat sodium concentration at the skin surface increases with sweat rate, ranging from ~20 mM at low sweat rates to ~100 mM at maximum sweat rate [13]. Although it is still partially controversial as to whether a linear relationship between sweat sodium concentrations and sweat rate exists, it's generally accepted that within a certain sweat rate ranges such linear relationships are present [13, 26]. In contrast, sweat potassium and urea concentrations, although not as extensively studied as sweat sodium, appear to be independent of sweat rate, most likely due to lack of re-adsorption mechanisms in the sweat duct [32, 33]. Because $[K^+]$ in measured sweat is expected to mirror plasma $[K^+]$ and remain consistent despite changes in sweat rate, sweat $[K^+]$ can be used as a quality control check of the sweat sample. If sweat $[K^+]$ is significantly above the normal range (*e.g.*, 10 mmol/L), potential issues with leaching or sample evaporation/contamination may be suspected [27].

Experimental (Sweat Monitoring Device Fabrication)

Integrated device for continuous sweat electrolyte monitoring: The sweat electrolyte monitoring device developed in this work is composed of three main modules (the sensor module, the microfluidics module and the electronics module) which are described in detail below.
Sensor Module: Ion Selective Electrodes: Over the past four decades, ion selective electrodes (ISEs) have been successfully used for the determination of both positive and negative ions in aqueous environments. More recently, these methodologies have been extended to measurements in physiological situations, such as blood plasma and sweat, to give information on electrolyte composition and concentration. Solid-state ISEs have focused on the replacement of solutions with solid-state reference electrodes. To fabricate the ISEs, a modified version of the protocol developed by Diamond's group [34] was implemented. The solid-state Na^+ and K^+ ISEs were based on the calix[4]arene tetraester Na^+ ionophore X and valinomycin, respectively. These ISEs, as well as the reference electrodes (RE) were fabricated using a 175 µm PET substrate onto which conducting carbon and dielectric insulating layers were screen-printed using a DEK 248 printer (See Figure 1-inset). A poly-3,4-ethylenedioxythiphene (PEDOT) solid-contact transducing layer was electrodeposited on the exposed carbon layer using 3,4-ethylenedioxythiophene (EDOT, 97% Sigma-Aldrich) and 1-ethyl-3-methylimidazolium bis(trifluoromethanesulfonylimide) [EMIM][NTf2] (Iolitec). To define the ISE and reference electrode membrane areas, two 3.0 mm diameter holes were laser cut in 500 µm PMMA which was then attached to the PET using an 86 µm pressure sensitive

adhesive film. To prepare the ISE membranes, 30 µL in total of the ion selective membrane cocktails based on 4-tert-butylcalix[4]arene-tetraacetic acid tetraethyl ester (Na^+) and valinomycin (K^+) were drop-cast on the solid-contact layer across several additions, allowing time for THF evaporation between each deposition. Similarly, for the reference electrode membrane, a cocktail consisting of the ionic liquid 1-hexyl-3-methylimidazolium tris-(pentafluoroethyl) trifluorophosphate (HMIM FAP), PMMA-co-BMA, and DEHP was dissolved in THF and drop-cast into the reservoir. The resulting combination electrodes were pre-conditioned for two hours in 0.01 M solutions of the relevant chloride salt.

The ISEs were calibrated using a high input-impedance multi-channel potentiometer (EMF-16, Lawson Labs) with a commercial double junction Ag/AgCl external reference electrode (Sigma Aldrich). Using solutions of NaCl and KCl increasing in concentration at decadal intervals from $1x10^{-4}$ M to $1x10^{-1}$ M, the potential response of the ISEs was recorded (See Figure 1-b for representative response of a Na^+ ISE). The initial response of the Na^+ and K^+ sensitive electrodes was slightly sub-Nernstian with an average slope of 54.852.9 ±5.8 mV/ log aNa^+ per decade Na^+ and 53.9 52.1±5.0 mV/log aK^+ per decade K^+ (N>25), respectively. Given the number of ionic species present in sweat, the realization of ISEs which discriminate against all ions other than that target ion is essential. In Figure 1-c), representative ISE response analysis in presence of interfering ions is shown, where the K^+ ISE shows no response to Na^+ ions in the concentration range of $1x10^{-4}$ M – $1x10^{-1}$ M, while its sensitivity to potassium ions is retained in an environment with more than one cationic species present.

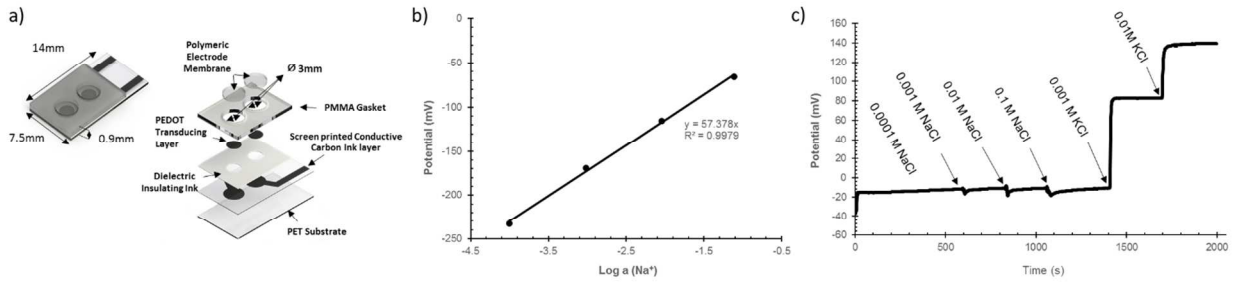

Figure 1: a) *The individual components of the ISE electrode (A) Polymeric electrode membrane (B) PMMA Gasket, (C) PEDOT transducing layer (D) Dielectric insulating ink (E) Screen printed conductive carbon ink layer (F) PET substrate and (G) The assembled ISE.* ***b)*** *Average response of a Na^+ ISE to changes in NaCl activity,* ***c)*** *Selectivity of K^+ ISEs in an Na^+ environment*

It should be noted that the sub-Nernstian response of the ISEs observed here differs from theoretical values due to non-ideal fluxes in the membrane. In solid state ISEs, this effect is exacerbated due to the non-symmetrical nature of the membrane with only an outer aqueous boundary in contact with the analyte. When exposed to high concentrations of perm-selective ions (Na^+ or K^+), the membrane concentration of the perm-ion gradually rises as there is no ion exchange at the internal boundary to remove this build up. This, in turn, gradually saturates the membrane and the condition that most of the calixarene receptors are free begins to break down, resulting in a drop in the membrane sensitivity (decreased slope). This is why, when we condition the membranes in pure water for up to 24 hours, we see the membrane potential gradually drifting towards lower values, and the sensitivity re-established to a large extent.

The microfluidics module: The fluid-handling portion of the device may be broken down into three sections: 1) the skin interface 2) the sensor interface and 3) the wick. To enable wicking of fluid into the channels, we have used laminated microfluidics formed from one or more hydrophilically-treated plastic films with patterned adhesives. In this additive technique, a cutting plotter is used to pattern each layer,

followed by lamination. This technique allows for rapid prototyping and implementation of channel geometry changes without the need for pattern-dedicated tooling (e.g., masks, stamps) or curing. Compared to laser cutting, this method leaves no debris or hydrophobic residue on the sides of the cut channel wall. Furthermore, this method is scalable to manufacturing with dedicated punches after the design is finalized.

The key physiological parameter which defined the device design was sweat rate. Sweat rate varies dramatically with physical activity, temperature, gender, skin location, and physiologic status among other variables [27].We have chosen to focus on the middle to upper range of sweat rates as this is representative of the population at greatest risk for dehydration events. Thus, two physiologically relevant sweat rates (medium = 13µL/cm^2/hr., and high = 96µL/cm^2/hr.) were chosen. The volume of the sensor flow cell was equal to 1.1 µL (the electrode flow cell has a stadium oval geometry - two semicircles separated by a rectangle - of total length 7mm and width 3mm and a height of 50µm). To capture potential electrolyte concentration changes effectively, it was considered to have one volume exchange of the flow cell at least every 2-3 minutes. With the chosen sweat collection area of 6.6cm^2, and at medium sweat rates, a sweat volume of 85 µL is generated every hour, which corresponds to the flow cell volume being completely exchanged in less than a minute. The required wick capacity was calculated by considering the amount of sweat generated at high sweat rate over six hours, which is approximately 3.8mL (6.6cm^2 x 96µL/hr. x 6 hrs.).

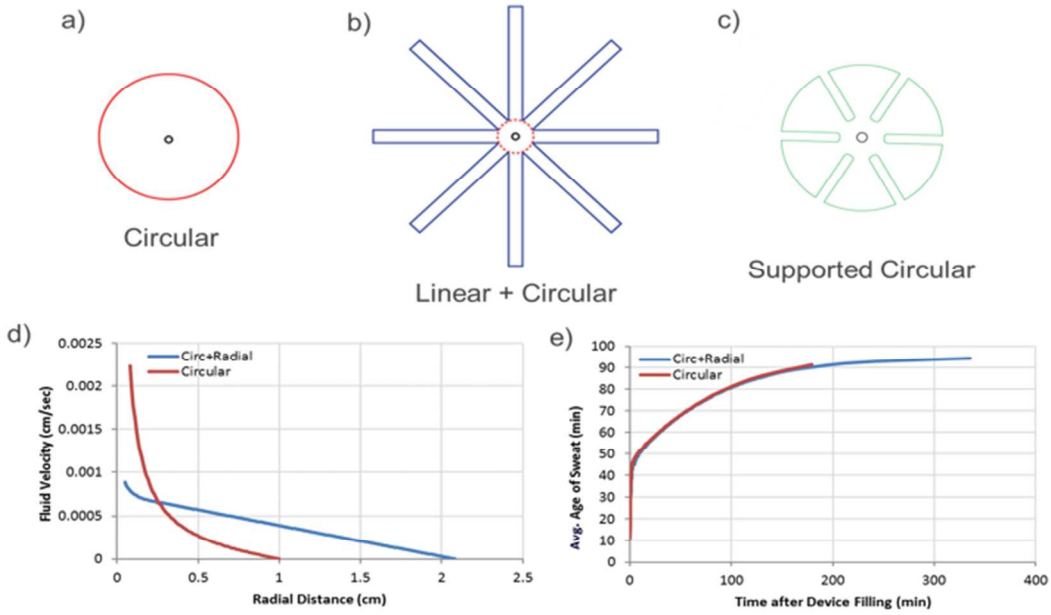

Figure 2: a-c) *Schematic designs of circular (red), spoked radial (blue) and hybrid supported circular (green) skin interface shapes of the same surface area.* ***d)*** *Modeling results of lateral sweat velocity as a function of radial distance for designs* ***a*** *and* ***b.*** ***e)*** *Average time since excretion for sweat generated in the designs shown as a function of time after sensor activation – note that all values are calculated for a "medium" sweat rate of 13µL/cm^2/hr. Calculated values scale as the linear inverse of the sweat rate.*

Based on the collection area defined above, the most obvious shape is a circular contour with a central aperture to channel the sweat from the whole area to the sensor (Figure 2-a)). We determined that a sweat collector covering a surface area of 0.9cm^2 (1.07cm diameter) would be sufficient to pass one volume of sweat, i.e.1.1 µL, in less than a minute through the sensor at the 96µL/cm^2/hr. sweat rate. A 6.6cm^2 sweat

collection area (2.9cm diameter) would be required at the lower 13µL/cm^2/hr. sweat rate. One potential drawback of a large diameter circle is that it is difficult to control the gap between skin and device over such an area. An increase in skin-film gap requires larger amounts of sweat to fill the collection volume and can cause variations in filling time. We considered an alternative spoked design of equivalent area consisting of rectangles running radially out from the collection point, overlapping in a central circle (Figure 2-b). A model was developed to explore the dynamics of sweat in both devices and specifically to understand the relative velocities and ages of the sweat in the device. The circular design was modeled homogeneously and the spoked design was modeled as a hybrid of linear (blue, Figure 2-b) and circular (dashed red circle, Figure 2-b) flows using the output of the linear model as the boundary conditions for the circular model. The output of this modeling showed that while the sweat velocity (radially inwards) increased for the circular design (Figure 2-d), the net effect on the average time excreted sweat took to reach the sensor was minimally changed by altering the design (Figure 2-e). We thus proposed a hybrid design (Figure 2-c) which uses minimal adhesive area to maintain the skin-device gap constant while limiting the overall device size.

One of the key learnings from this exercise was that there can be a long lag time required to fill the device with sweat to begin sensing (e.g., 46 minutes at the 13µL/cm^2/hr. sweat rate for a circular collection area- See Supplementary Section A), which motivated us to minimize the dead volume of the device, both by minimizing the fluidic volume in the device, as well as by minimizing the skin-to-sweat collector gap. Even with adhesives of minimal thickness (e.g., 25µm), the inherent roughness of skin makes it difficult to reliably achieve gap heights of less than 100µm (assuming shaved skin).

Dimensions of the disposable patch: 4.15”x3.85” (including the holder tab)

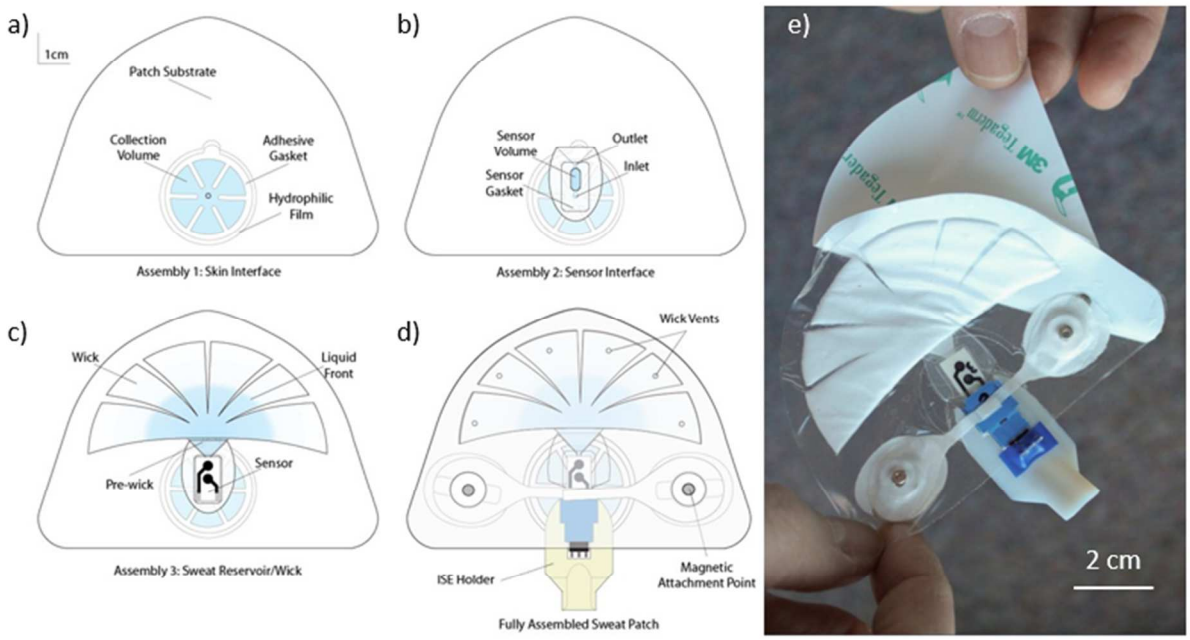

Figure 3: Microfluidics module: a) *Sweat collection and skin interface,* ***b)*** *Fluidics and Sensor Gasket,* ***c)*** *Sweat reservoir/wick.* ***d)*** *Schematic of fully assembled sweat patch consisting of microfluidics and ISE sensor components.* ***e)*** *Representative image of fully assembled sweat patch. Dimensions of the disposable patch: 10.5cm x 9.7cm*

Beginning at the skin, the first layers of the device comprise the circular skin interface made up of a thin, patterned adhesive and a circular hydrophilic film adhered to the patch substrate (see Figure 3-a). Next, a second patterned adhesive layer defines the fluidic channel which carries sweat from the inlet past the sensor chip towards the wick on the downstream side (see Figure 3-b). The geometry of this section is defined by the size of the ISE sensor (two circular electrodes separated by a small gap). In this volume, a glass fiber wick is placed to ensure rapid and even distribution of liquid across the two electrodes and prevent air bubbles from being retained in the channel.

The third and final section of the device provides an outlet for the collected sweat and attempts to maintain a consistent flux of sweat (Figure 3-c). Our initial designs were conceived based on fiber-based materials (cellulosic and similar materials) using capillary force to wick the incoming sweat into pores, though alternatives including hydrogels and highly absorbent polymers such as sodium salts of polyacrylic acid may be considered for long duration, high sweat rate applications. One of the critical characteristics of a wick for this application is the flow rate, specifically having a very low flow rate compared to traditional cellulosic materials to avoid outpacing the input rate of the sweat released by the body. As shown in Figure 3-c), a fan-shaped wick design was chosen to allow motion of the separate "digits" of the wick during use, while maintaining a large fluid reservoir area. Because of the thickness of the wick (0.625mm), a small Whatmann Standard 17 "pre-wick" was incorporated to transfer fluid from the fluidic channel to the reservoir. (Details of wick material down-selection and testing are provided in Supplementary Section B.)

The electronics and energy module: A custom data acquisition and Bluetooth transfer board developed for Dublin City University's Sweatch sodium ion measurement system by Shimmer™ was used to interrogate the ISEs [17]. The main challenge in integrating the Shimmer™ board was to design an enclosure with appropriate support for the rigid PCB along with a reasonably flexible interface to the flexible microfluidics module to allow the full device to move comfortably with the user. Furthermore, a thorough investigation of the sweat sensor patch in use revealed several potential noise sources which are susceptible to external mechanical stimuli. The first versions of the 3D printed Shimmer PCB case was made entirely from a flexible/stretchable resin (Stratasys TangoPlus FLX930). While this package was sufficient to prevent damage to the board in normal use, the limited stiffness of the TangoPlus FLX material allowed some mechanical strains to be transmitted to the Shimmer™ board within. In particular, pressure against the back plane of the board (skin-side) caused reproducible offsets on the order of 50-100 mV, and torsion of the encased device similarly caused shifts in the read-out of the sensor. To address both phenomena, internal rigidification of the electronics module was undertaken. Specifically, an internal skeleton made from rigid plastic (Stratasys VeroClear-RGD810/VeroWhitePlus-RGD835) was designed to mate to the shimmer board with a super-structure to prevent battery motion and allow space for the connection of the ISE. Further, to prevent back-plane pressure, a thin aluminum plate was placed below the skeleton. To create a direct stabilized connection from the ISE to the board, the Shimmer case and skeleton were modified to incorporate a 3-pin, 0.1in spacing female connector directly bonded to the skeleton. The outer two pins of this connector were wired into the ISE and reference electrode inputs on the board via a wire chase built into the skeleton to prevent wire motion. Additionally, a cut-away was built into the bottom of the Shimmer case to allow space for the connection hardware and prevent contact with the ISE during use. In Figure 4 a) - f), the electronics module and the assembled device are shown. Magnetic snaps (0.4" diameter) were used to fasten the electronics module to the patch, and were wired to allow battery charging of the enclosed device.

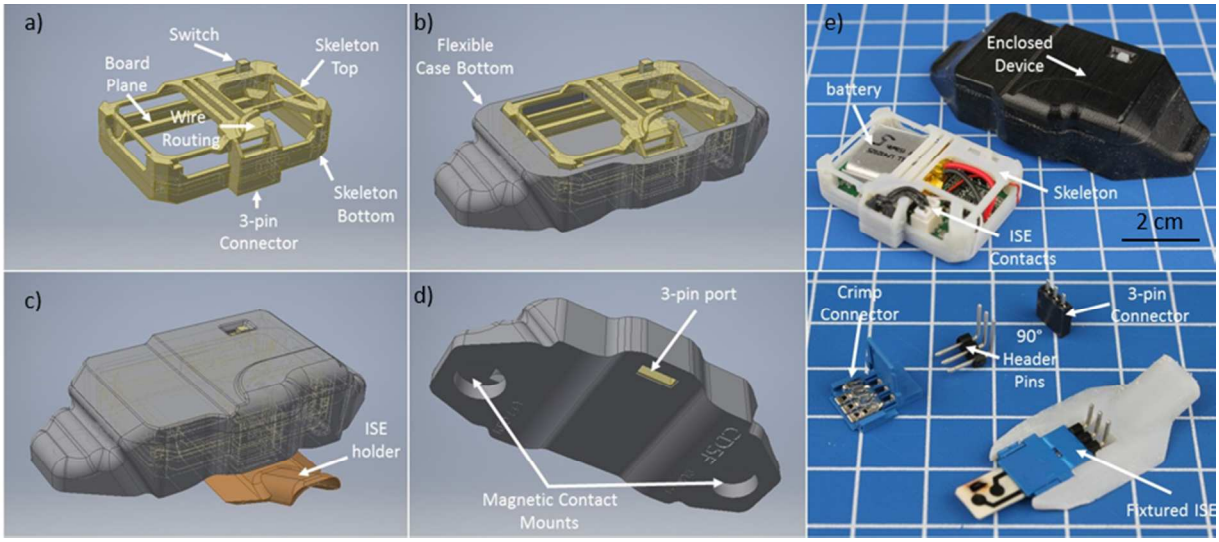

Figure 4: Electronics module enclosure: a) *Skeleton with a 3-pin header connection wired out the bottom of the device (and bound to the skeleton), wire-chase to prevent wire motion, and easier access to the ISE connection plug on the Shimmer board.* ***(b-d)*** *flexible enclosure with magnetic connectors at the ends of the device and a cut-out on the bottom to allow space for the crimp connector and prevent motion artifacts from contact with the ISE in the patch.* ***e)*** *Photograph of new ISE connection assembly, Shimmer electronics module (lower right) and assembled module (upper right).* ***f)*** *Representative image of the fully integrated sweat sensing device. Dimensions of the fully packaged electronics module: length= 7.6 cm, width= 3.5 cm and thickness= 1.7cm.*

Results and Discussion

Performance of the sweat electrolyte monitoring device: The performance of the integrated wearable sweat monitoring device was evaluated in both laboratory and field settings. On-body, functional testing of a sweat patch sensor system is invaluable to determining suitability for use, but is not sufficient for device development for two main reasons. First, sweat ion concentration and rate cannot be readily or reproducibly controlled or varied, and second, a myriad of noise sources and interferences are possible when a subject is rapidly moving while generating sweat. Thus, it is beneficial to test sweat sensors under model conditions where the sweat composition and rate can be varied controllably and motion and environmental artifacts can be controlled. A fluidic system for artificial sweat delivery to the patch was developed and used to troubleshoot the sweat patch design (See Supplementary Section C).

The first laboratory tests focused on the effects of incorporating a sweat sensor (sodium-sensitive ISE) into the patch assembly. Thus, a partial patch was constructed which left the ISE exposed while incorporating other components of the fluidic path including the glass fiber wick/spreader. Aliquots of the desired concentrations of aqueous Na^+ were then drop-wise added and wicked off with an absorbent wipe and compared to performance outside the patch. The results of this testing are shown in Figure 5 a). The performance of the ISE in these two conditions is functionally similar and shows that the material composition of the fluidics contacting the ISE do not interfere with its ability to sense Na^+. The difference at the outset is due to different amounts of residual salt from previous testing and is recovered after equilibration with the calibration solutions.

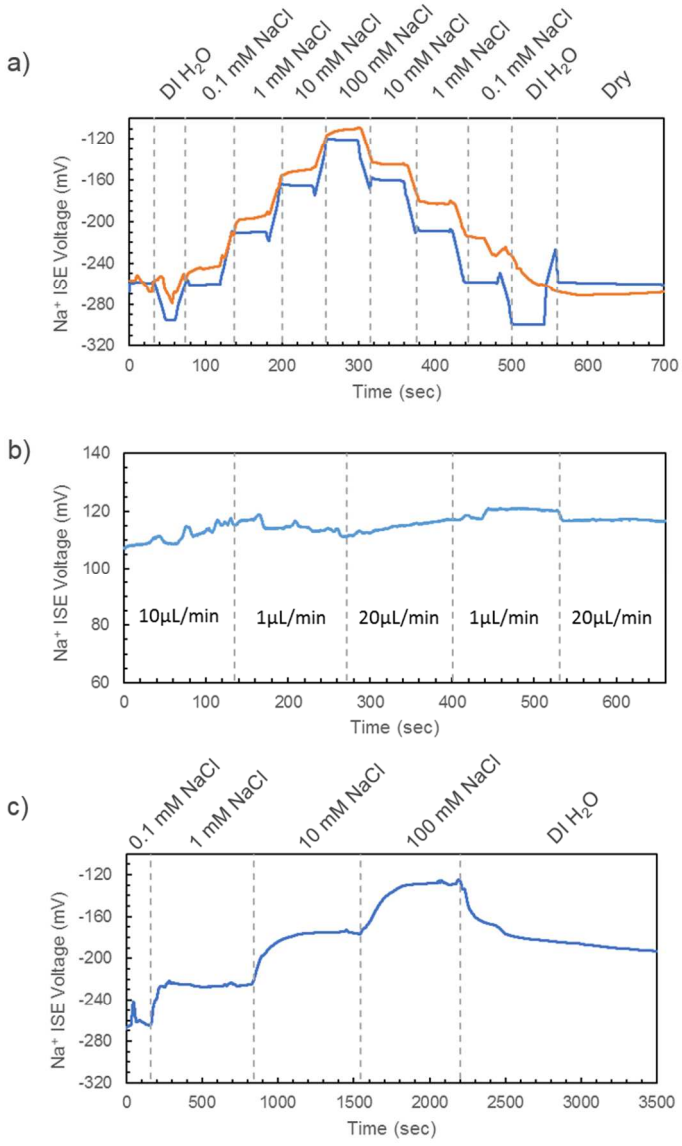

Figure 5*: a) Representative response of a Na^+ ISE to changes in NaCl concentrations as a stand-alone sensor and when embedded in the microfluidics patch. In the case of the stand-alone ISE, the analyte was removed from the sensing site by bringing a wicking cloth in close contact to the surface of the sensor. When the ISE is embedded in the microfluidics patch, the fluid removal from the sensing site takes place automatically. b) Representative response of an integrated sweat sensor to changes in flow rate (A 100 mM NaCl salt solution was used). c) In patch flow experiments, elucidating the dynamic response of a Na^+ ISE to various salt concentrations at a flow rate of 5-10µL / min.*

Next, the performance of the integrated ISE and microfluidics patch under flow rates ranging from 1-20 µL/min was investigated under controlled laboratory conditions. In Figure 5-b), the response of a Na^+ ISE embedded in the fluidics patch to a constant salt concentration of 100 mM at varying flow rates is shown. In Figure 5-c), we show the dynamic response of a Na^+ ISE integrated in a patch to various salt solutions at a flow rate of 5-10µL/min., which is at the medium-high end of expected flow rates in this system on-body. The relatively slow equilibration times seen in these in-patch measurements are primarily due to the syringe pump feeding system, where a 2" long polymer tube is used between syringe containing solutions with sodium ions of a defined concentration and the sweat patch inlet area. When the syringe is

exchanged for one with a different concentration, the laminar flow in the tube combined with shear along the tube walls leads to mixing of the previous solution with the new one. This may be addressed by minimizing the hold-up volume of the system as a whole but is inherent to the test set up system used here. When the sweat patch is used on the body, this effect does not occur and any "peak broadening", or loss in temporal resolution is due only to the sweat mixing/retention in the inlet area and in the short channel section (2mm long) between the channel inlet and the ISE location. The specific requirements for the temporal resolution of sweat sensing devices are not well-established and vary as a function of end use. However, we believe a temporal resolution of ~10 minutes might be adequate for the target hydration monitoring applications. For instance, total body water studies, using meticulous labeling protocols, have shown that the time required between the consumption of a glass of labelled water and its detection in sweat is about 7-10 minutes. Enhanced temporal resolution capabilities in sweat sensing devices may render benefits beyond prevention of new and old sweat mixing. For example, rapid transport of sweat from the secretion site to the wicking reservoir, at least partially, reduces prolonged water induced skin occlusions that may result in undesired effects such as hydromoesis. If the sweat is removed rapidly from the skin surface, the re-absorption of sodium by the sweat glands is decreased. This potential benefit is more significant at higher sweat rates. In a control study, we have also shown that rapid fluid transport and its in-situ analysis capabilities may play a significant role in preserving the initial sweat composition, i.e., immediately after secretion from the eccrine glands. For example, we observed substantial changes in the potential of a stand-alone Na^+ ISE (which did not include the microfluidics module) exposed to a 0.01M NaCl solution over a one-hour period. In this case, the salt solution was delivered through a skin-mimicking porous rayon film interface of 50 µm thickness, which was bought in direct contact to the ISE surface, and the observed variations in the sensor response could be attributed to undesired evaporation effects (See Supplementary Section D). The evaporation caused an increase in the electrolyte concentration, causing the sensor to read a sodium concentration that was higher than that of the original sample. Beyond electrolytes, alterations in the composition and concentration of other sweat solutes, such as small proteins, could be more significant due to time sensitive enzymatic degradation. It is therefore likely that wearable sensors which remove the sweat from the skin surface immediately can offer a more accurate reading of analytes than those that rely on direct skin contact.

On-body testing of the fully integrated sweat sensors was performed with a healthy male volunteer (Informed consent was obtained) during high intensity exercise on a bicycle on a roller trainer (to allow for and encourage realistic motion of the subject) and during treadmill running trials (Figures 6-a) and 6-b)). The patches were located on the subject's back, adjacent to the spine on the latissimus dorsi muscle and/or thoracolumbar fascia in the region of the upper lumbar vertebra. This site was chosen for its combination of a reasonably high sweat rate, with a limited range of motion during cycling or other activities (compared to e.g., extremities). Also, in this position the device is quite unobtrusive for activities which do not require the use of a backpack or other equipment which might impinge on the lower back.

The average speed during biking was between 26 and 29 mph for the duration of the session, typically 30 to 60 minutes, leading to profuse sweating in the individual undergoing testing. At the end of one session, a brief treadmill workout was included to test the device under harsher conditions of movement compared to the relatively static biking position. The subject ran for approximately ten minutes on a treadmill at speeds between 8 and 10 mph to test the noise response of the system as a function of exertion and tempo. The sweat patch and associated electronics module were monitored remotely via Bluetooth for the duration of the exercise sessions. The drift in the signal due to electronics noise and connection to the patch itself under cycling or running motions is in the order of 3mV per 30 minutes, while the average random noise (millisecond-second timescale) is on the order of <1mV with several larger excursions (<3

mV). Thus, based on the oversampling of the Shimmer board (100Hz) with respect to changes in hydration status (minutes), we feel confident that no pertinent data is lost by using a noise suppression algorithm such as a 15 second moving average. In Figures 6-d), the outputs of fully integrated Na^+ (the upper panel) and K^+ (lower panel) patches during a biking trial are shown. In this particular experiment, the sensitivity of the Na^+ and K^+ ISEs were equal to 55.73.8mV/ log a Na^+ and ~53.92.0mV/log a K^+ per decade for the corresponding ion concentrations, respectively. For the Na^+ concentration, the results in Figure 6-d) show the expected rise in voltage corresponding to the introduction of eutonic sweat to the ISE (from a dry baseline) with minimal noise aberrations. Figure 6 e-f show infrared imaging of a subject during an exercise trial. The infrared imaging shows the temperature distribution across the subject's back (orange/white = high heat, purple/blue = low temperature). There is some evidence of localized heating in the vicinity of the of the sweat patch which is attributable to the insulating and blockings effects of placing material over the skin. Figure 6 f shows a magnified view of the sensor patch itself, highlighting the temperature decreases found at the wick outlets where the sweat is allowed to evaporate, showing that sweat is flowing completely through the device.

The primary focus of this work was the development and optimization of the sensor system rather than its clinical application. Thus, all work was carried out under a scope of work which was determined not to be human subject testing (E&I Institutional Review Board). As a result of this process, the data collected during on-body was specifically not calibrated to prevent the generation of physiologic data on the subject, thus all data for on-body testing is presented in the raw form (mV). Based on representative calibrations performed in bench testing, the data collected fall within the expected physiologic ranges for perspiration. Future testing of the device under conditions of controlled hydration and dehydration are planned to further assess the clinical utility of real-time electrolyte monitoring as it relates to gold-standard hydration metrics (weight, urine and plasma osmolality, etc.).

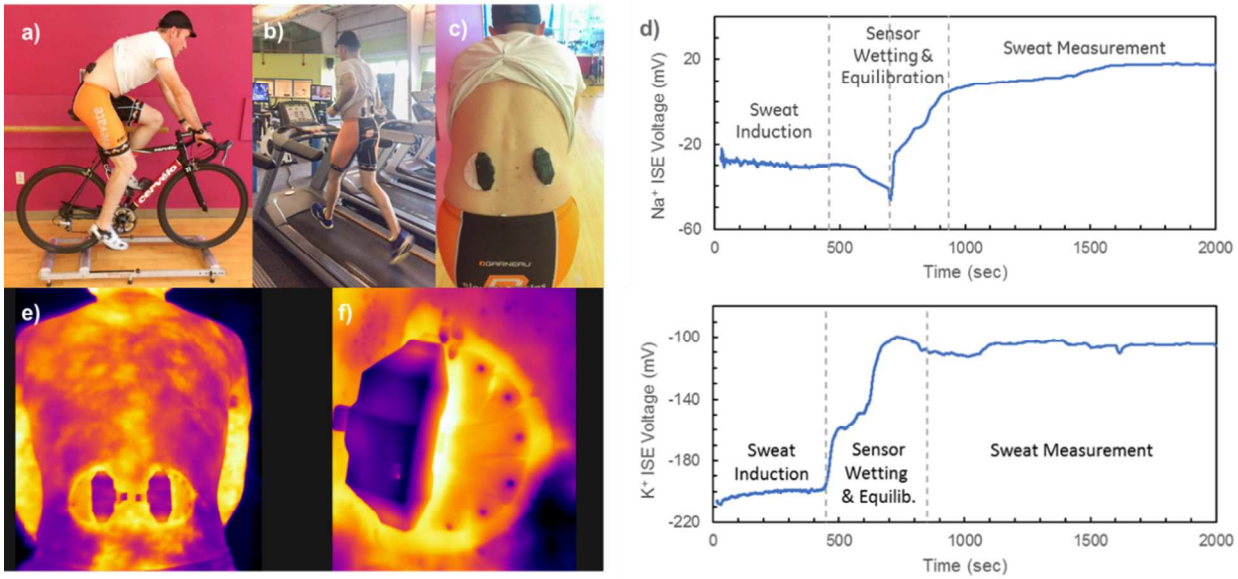

Figure 6: On-body test results: *Testing of the integrated sweat sensor during biking* ***(a)*** *and running* ***(b)*** ***trials.*** ***(c)*** *Images of sweat patches and electronics units on a subject's back* ***(d)*** *Integrated sweat patch outputs during a biking trial including a Na^+-sensitive patch (top) and a K^+-sensitive patch (bottom) based on measurements of sweat generated by the subject.* ***(e)*** *Infrared imaging of patches on a subject's back, showing heat distribution across*

subject. (f) close-up infrared image of patch & electronics unit showing cooling effect of sweat evaporation at the outlet holes (purple dots at periphery of patch).

Conclusions

In summary, we have successfully demonstrated a wireless sweat monitoring device that offers a unique combination of user comfort, high accuracy and continuous and non-obtrusive sweat electrolyte monitoring over extended periods of time. This device is composed of a highly flexible, disposable sensor/microfluidics module and a reusable electronics module, making it highly adaptable and suitable for continuous Na^+ and K^+ balance assessment during athletic or military training applications. The key differentiating features of the device presented here include: 1- a fluidics system that simultaneously allows for effective sweat collection from the skin at moderate to high perspiration rates (while minimizing sensor lag) and rapid removal of sweat from the sensing site (to minimize hydromeiotic effects); 2- a highly engineered electronics module housing, overall device integration schemes and signal processing algorithms that allow for a very low noise yet comfortable to wear system. The sweat monitoring device presented here was laboratory tested with simulated sweat by the GE Global Research Team. Additional physiological performance testing occurred at the AFRL 711th Human Performance Wing's Signature Tracking for Optimized Nutrition and Training Laboratory. Furthermore, a field test of the device took place in March 2018 in Colorado Springs through a collaboration between the AFRL's Materials and Manufacturing Directorate, the 711th Human Performance Wing and U.S. Air Force Academy cadets[35]. The multi-day testing event at the Air Force Academy provided key information on the ability of the wearable sweat monitoring device to perform in a relevant military training environment. Academy cadets wore the sweat sensing device during a three-hour workout that included a run through the academy obstacle course, a one-and-one-half mile ruck march and a series of callisthenic exercises that included pull-ups, push-ups and sit-ups. Field applications, such as athletic/ military training in complex environments and first responder safety while actively addressing fire or chem-biological hazardous events, will require highly non-obtrusive, accurate, in-situ and continuous monitoring capabilities, for which the sweat monitoring system presented here is highly adequate. Meanwhile, in circumstances where sporadic and more qualitative knowledge of sweat composition or volume are desired, colorimetric assays may suffice. On-going research by our groups is focused on the development of the second generation of the wearable sweat monitoring device to further improve their reliability for realistic operations, increase the shelf-life and stability of potentiometric sensors, reduce their footprint and incorporate additional sweat assessment capabilities such as sweat rate sensing. Controlled exercise trials are also being conducted to assess sweat volume and electrolyte concentrations at various levels of hydration to establish physiologically relevant correlations.

Acknowledgements

The Nano-Bio-Manufacturing Consortium, NextFlex (the USA Manufacturing Institute for Flexible Hybrid Electronics) and the Air Force Research Laboratory are acknowledged for financial support. The authors are very thankful to Dr. Larisa Florea and Dr. Colm Delaney of Dublin City University, and Dr. Nandini Nagraj for valuable discussions and their assistance with this work. Dr Malcolm Thompson, Dr. Melissa Grupen-Shemansky, Laura Rae, Laura Sowards, Dr. Jeremy Ward and Dr. Benjamin Leever are thanked for their encouragement and making this program possible. The views and conclusions contained herein are those of the author(s) and should not be interpreted as necessarily representing the official policies or endorsements, either expressed or implied, of Air Force Research Laboratory or the U.S. Government.

References

1. D. J. Casa, L. E. Armstrong, S. K. Hillman, S. J. Montain, R. V. Reiff, B. S. Rich, W. O. Roberts and J. A. Stone, *Journal of athletic training*, 2000, **35**, 212.
2. M. N. Sawka, A. J. Young, R. P. Francesconi, S. R. Muza and K. B. Pandolf, *Journal of Applied Physiology*, 1985, **59**, 1394-1401.
3. F. M. Williams-Bell, B. Aisbett, B. A. Murphy and B. Larsen, *Frontiers in physiology*, 2017, **8**, 815.
4. H. R. Lieberman, *Journal of the American College of Nutrition*, 2007, **26**, 555S-561S.
5. A. C. Grandjean and N. R. Grandjean, *Journal of the American College of Nutrition*, 2007, **26**, 549S-554S.
6. K. E. D'Anci, F. Constant and I. H. Rosenberg, *Nutrition reviews*, 2006, **64**, 457-464.
7. R. W. Kenefick, S. N. Cheuvront, L. Leon and K. K. O'Brien, *Dehydration and rehydration*, ARMY RESEARCH INST OF ENVIRONMENTAL MEDICINE NATICK MA THERMAL AND MOUNTAIN MEDICINE DIVISION, 2012.
8. C. Munoz, E. Johnson, J. Demartini, R. Huggins, A. McKenzie, D. Casa, C. Maresh and L. Armstrong, *European journal of clinical nutrition*, 2013, **67**, 1257-1263.
9. S. N. Cheuvront and R. W. Kenefick, *Comprehensive Physiology*, 2014.
10. A. Pai, K. Cardone, R. Daoui, P. Salenger, X. Chen, T. Kao, G. Boverman and D. Davenport, 2015.
11. X. Chen, T.-J. Kao, J. M. Ashe, G. Boverman, J. E. Sabatini and D. M. Davenport, *Physiological measurement*, 2014, **35**, 1137.
12. Z. Sonner, E. Wilder, T. Gaillard, G. Kasting and J. Heikenfeld, *Lab on a Chip*, 2017, **17**, 2550-2560.
13. D. P. Rose, M. E. Ratterman, D. K. Griffin, L. Hou, N. Kelley-Loughnane, R. R. Naik, J. A. Hagen, I. Papautsky and J. C. Heikenfeld, *IEEE Transactions on Biomedical Engineering*, 2015, **62**, 1457-1465.
14. G. Matzeu, C. O'Quigley, E. McNamara, C. Zuliani, C. Fay, T. Glennon and D. Diamond, *Analytical Methods*, 2016, **8**, 64-71.
15. A. Koh, D. Kang, Y. Xue, S. Lee, R. M. Pielak, J. Kim, T. Hwang, S. Min, A. Banks and P. Bastien, *Science translational medicine*, 2016, **8**, 366ra165-366ra165.
16. S. Imani, A. J. Bandodkar, A. V. Mohan, R. Kumar, S. Yu, J. Wang and P. P. Mercier, *Nature communications*, 2016, **7**, ncomms11650.
17. T. Glennon, C. O'Quigley, M. McCaul, G. Matzeu, S. Beirne, G. G. Wallace, F. Stroiescu, N. O'Mahoney, P. White and D. Diamond, *Electroanalysis*, 2016, **28**, 1283-1289.
18. W. Gao, S. Emaminejad, H. Y. Y. Nyein, S. Challa, K. Chen, A. Peck, H. M. Fahad, H. Ota, H. Shiraki and D. Kiriya, *Nature*, 2016, **529**, 509-514.
19. S. Emaminejad, W. Gao, E. Wu, Z. A. Davies, H. Y. Y. Nyein, S. Challa, S. P. Ryan, H. M. Fahad, K. Chen and Z. Shahpar, *Proceedings of the National Academy of Sciences*, 2017, 201701740.
20. J. Choi, D. Kang, S. Han, S. B. Kim and J. A. Rogers, *Advanced healthcare materials*, 2017, **6**.
21. A. J. Bandodkar, D. Molinnus, O. Mirza, T. Guinovart, J. R. Windmiller, G. Valdés-Ramírez, F. J. Andrade, M. J. Schöning and J. Wang, *Biosensors and bioelectronics*, 2014, **54**, 603-609.
22. H. Y. Y. Nyein, L.-C. Tai, Q. P. Ngo, M. Chao, G. B. Zhang, W. Gao, M. Bariya, J. Bullock, H. Kim, H. M. Fahad and A. Javey, *ACS Sensors*, 2018, **3**, 944-952.
23. A. Martín, J. Kim, J. F. Kurniawan, J. R. Sempionatto, J. R. Moreto, G. Tang, A. S. Campbell, A. Shin, M. Y. Lee, X. Liu and J. Wang, *ACS Sensors*, 2017, **2**, 1860-1868.
24. M. McCaul, T. Glennon and D. Diamond, *Current Opinion in Electrochemistry*, 2017.
25. J. Heikenfeld, *Electroanalysis*, 2016, **28**, 1242-1249.

26. M. J. Buono, K. D. Ball and F. W. Kolkhorst, *Journal of Applied Physiology*, 2007, **103**, 990-994.
27. L. B. Baker, *Sports Medicine*, 2017, 1-18.
28. C. J. Smith and G. Havenith, *European journal of applied physiology*, 2011, **111**, 1391-1404.
29. C. E. Dziedzic, M. L. Ross, G. J. Slater and L. M. Burke, *International journal of sports physiology and performance*, 2014, **9**, 832-838.
30. D. Brebner and D. M. Kerslake, *The Journal of physiology*, 1964, **175**, 295-302.
31. K. Sato, W. Kang, K. Saga and K. Sato, *Journal of the American Academy of Dermatology*, 1989, **20**, 537-563.
32. K. Sato, *American Journal of Physiology--Legacy Content*, 1973, **225**, 1147-1152.
33. T. C. Boysen, S. Yanagawa, F. Sato and K. Sato, *Journal of Applied Physiology*, 1984, **56**, 1302-1307.
34. D. Diamond, G. Svehla, E. Seward and M. McKervey, *Analytica chimica acta*, 1988, **204**, 223-231.
35. M. Alia-Novobilski, *Wright Patterson Air Force Base Press Release*, 2018, http://www.wpafb.af.mil/News/Article-Display/Article/1495074/afrl-led-patches-make-sense-of-sweat/